Physica E 121 (2020) 113830

Contents lists available at ScienceDirect

Physica E: Low-dimensional Systems and Nanostructures

journal homepage: http://www.elsevier.com/locate/physe

Process optimization for green synthesis of gold nanoparticles mediated by extract of *Hygrophila spinosa* T. Anders and their biological applications

Swaha Satpathy [a,b], Arjun Patra [a,b], Bharti Ahirwar [b], Muhammad Delwar Hussain [a,*]

[a] Department of Pharmaceutical & Biomedical Sciences, College of Pharmacy, California Health Sciences University, Clovis, 93612, California, USA
[b] Institute of Pharmacy, Guru Ghasidas University, Bilaspur, 495009, Chhattisgarh, India

ARTICLE INFO

Keywords:
Green synthesis
Gold nanoparticles
Hygrophila spinosa
Anticancer
Antioxidant

ABSTRACT

Plant extract-mediated green synthesis of gold nanoparticles (AuNPs) and their biomedical application is currently gaining huge interest in the field of nanotechnology. In the present study, AuNPs were synthesized using *Hygrophila spinosa* aqueous extract (HSAE). The formation of AuNPs was confirmed by observing color change and characteristic absorbance peak for surface plasmon resonance by UV–Vis spectroscopy. Different reaction parameters such as HSAE concentration, salt concentration, pH, reaction time and temperature were optimized for biosynthesis of AuNPs. The NPs were characterized for particle size, surface morphology, crystallinity, elemental composition and surface functionalities. Cytotoxicity of the AuNPs was studied against different cancer cell lines by MTT assay and antioxidant potential as total antioxidant capacity was also evaluated. The biosynthesized AuNPs were small in size and negatively charged. Phytochemical screening of HSAE, and FTIR spectrum of synthesized AuNPs demonstrated participation of various groups of chemical compounds as capping and stabilizing agents in biosynthesis of AuNPs. The green synthesized AuNPs exhibited significantly higher anticancer activity compared to HSAE against breast, ovarian, glioblastoma/brain and multi-drug resistant ovarian cancer cell lines. Antioxidant activity of the synthesized AuNPs was less than HSAE. The biosynthesized AuNPs could be studied further to access their potency in the treatment and imaging of various cancers.

1. Introduction

Nanotechnology deals with design, manipulation, preparation and application of materials in nanometer range with their application in diverse fields such as biomedical, food, agriculture, drug delivery, cosmetics, energy, textile etc [1–3]. In recent years, nanoparticle (NPs) synthesis has been of great research interest because of their excellent biomedical applications, electronic, optical and chemical properties [4,5]. Metallic NPs have been synthesized by chemical and physical methods using different metals such as Ag, Au, Cu and Zn. Among these NPs, gold NPs (AuNPs) have gained significant attention due to their application in cancer therapy and imaging, angiogenesis, genetic disease and genetic disorder diagnosis, photothermal therapy and photoimaging [6,7]. AuNPs have been designed for specific delivery of anticancer agents like paclitaxel, doxorubicin and methotrexate [8]. Chemical methods are the most popular approach for synthesis of metallic NPs which are based on the reduction of metallic ion solutions with reducing and capping agents such as sodium citrate, sodium borohydride, trisodium citrates, *N*,*N*-dimethyl formamide, 2-mercaptobenzimidazole, sodium hydroxide and sodium dodecyl sulfate [9,10]. Many of these materials used during the synthesis are harmful to both human health and the environment. In addition, these NPs are not suitable for biomedical application [11]. Green nanotechnology which is eco-friendly thus opens various opportunities for designing nanomaterials for biomedical application [12,13]. The green approach of metal nanoparticle synthesis has various advantages compared to conventional methods such as (i) biocompatibility and significant application in biology and medicine, (ii) simplicity of the method, (iii) Use of natural resources (microorganisms, algae, fungi, plants), (iv) non-toxic method making the synthesized NPs suitable for pharmaceutical and biomedical applications, (v) external capping or stabilizing agents are not needed for synthesis of NPs, (vi) cost effective method because of minimum or non-requirement of energy, (vii) simplicity in scaling up for large-scale synthesis, (viii) reproducibility in production, (ix) well defined morphology of synthesized NPs [1,14–19].

The phytoconstituents of plants such as flavonoids, phenolics,

* Corresponding author.
E-mail address: dhussain@chsu.edu (M.D. Hussain).

https://doi.org/10.1016/j.physe.2019.113830
Received 21 March 2019; Received in revised form 7 October 2019; Accepted 18 November 2019
Available online 22 November 2019

Table 1
Preliminary phytochemical screening of HSAE.

Chemical class	HSAE
Alkaloids	–
Glycosides	–
Carbohydrates	+
Saponins	–
Phytosterols	–
Tannins and polyphenolics	+
Proteins	+
Amino acids	+
Gums and mucilage	+
Flavonoids	+

+, present; -, absent; HSAE, *Hygrophila spinosa* aqueous extract.

carbohydrates and proteins have the capability of reducing the metals from their higher oxidation to zero oxidation state [20,21]. The metallic precursor converts into their respective NPs by the antioxidant potential of the phytoconstituents which acts as reservoir of electrons and in turn the NPs are synthesized without use of hazardous and toxic reducing agents [22]. Plant mediated AuNPs have been extensively investigated in biomedical fields including drug delivery, tissue imaging, identification of clinical pathogens etc. The nanoparticles are synthesized by simply mixing aqueous chloroauric acid solution and plant extract where the phytoconstituents of the extract works as reducing and stabilizing agent. AuNPs using plant extracts has been synthesized, characterized and evaluated for various biological applications such as anticancer, antimicrobial, antioxidant, analgesic, sedative activities, but still a lot of research is in progress in this field owing to the diversity and potential of plants to produce NPs of different shapes [3,5,6,23–26].

The medicinal plant, *Hygrophila spinosa* T. Anders (Acanthaceae) commonly known as "Talmakhana" is listed in the Ayurvedic Pharmacopoeia of India. Leaves, roots, seeds, and whole plant of *H. spinosa* are traditionally used for management of a wide range of complications [27]. The plant comprises of alkaloids, carbohydrates, flavonoids, tannins and phenolics, steroids, proteins, organic acids and amino acids [28]. These secondary metabolites are mainly responsible in the formation of metal nanoparticles. The plant has been explored for different pharmacological activities [28–39] and contains several bioactive constituents [40–45].

Taking into consideration the wide range of secondary metabolites of the plant, in the present study, we report a simple, inexpensive and novel eco-friendly approach for biosynthesis of gold nanoparticles (AuNPs) using *H. spinosa* extract. Various reaction parameters such as plant extract concentration, reaction time and temperature, gold salt concentration and pH were optimized for synthesis of AuNPs. The synthesized AuNPs were characterized and evaluated for anticancer activity in different types of cancer and antioxidant potential.

2. Experimental

2.1. Collection and preparation of plant material

Fresh plants of *H. spinosa* were collected from Bilaspur, Chhattisgarh, India and authenticated through Indian Council of Agricultural Research-National Bureau of Plant Genetic Resources (ICAR-NBPGR), Regional Station, Phagli, Shimla, India (No.: NBPGR-565-569). The plant materials were cut into small pieces and shade dried for 15 days. The dried material was coarsely powdered and stored in air-tight container till further use.

2.2. Preparation of extract

Coarse powder material (100 g) was extracted by soxhlation with ethanol (95%, 300 mL). The ethanol extract was concentrated using rotary evaporator, dried and preserved in airtight container until further use. Five (5.0) g of the above extract was added to 100 mL of distilled water, sonicated for 5 min and filtered (Whatman filter paper, Sigma Aldrich). Further, the filtrate was again filtered through 0.22 μm cellulose acetate membrane filter (VWR International, USA) and the *H. spinosa* aqueous extract (HSAE) was kept in airtight container at 4 °C until further use.

2.3. Preliminary phytochemical screening (PPS)

The existence of different classes of chemical compounds like alkaloids (Mayer's test, Dragendorff's test, Hager's test and Wagner's test), glycosides (Keller Killiani test and Legal test), carbohydrates (Molisch's test), saponins (foam test), phytosterols and terpenoids (Libermann-Burchard Test), tannins and polyphenolics (ferric chloride test), proteins

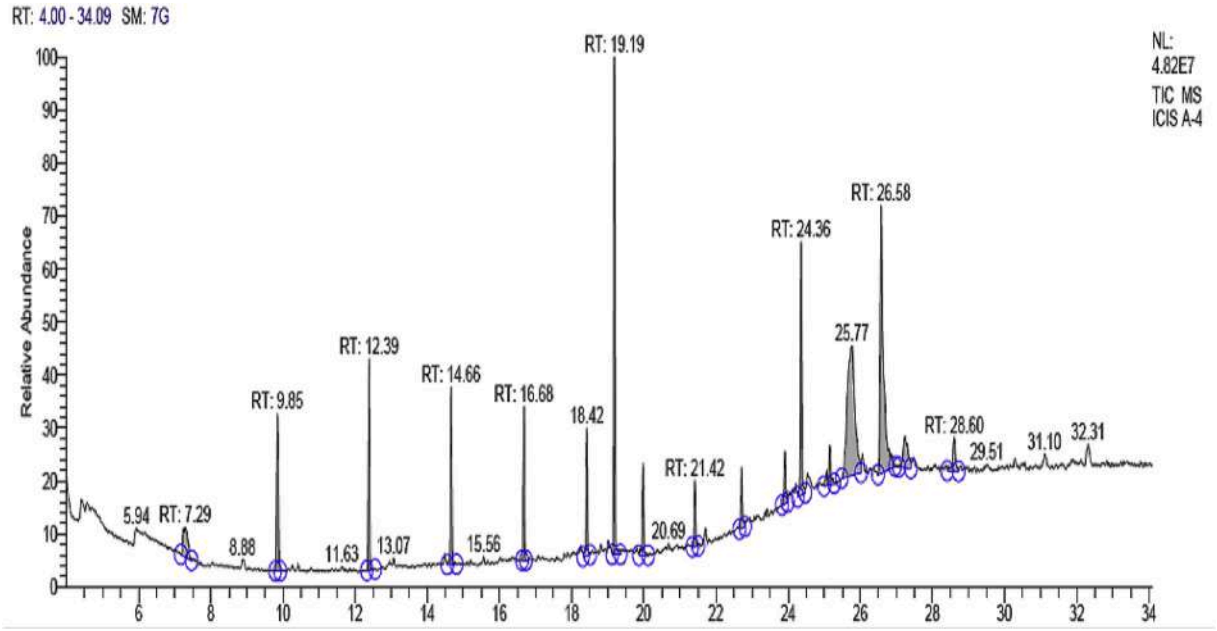

Fig. 1. GC/MS chromatogram of *H. spinosa* aqueous extract (HSAE).

Table 2
Different chemical constituents in *H. spinosa* aqueous extract by GC/MS.

Serial No.	Peak RT (min)	Compound identified	Molecular formula	Chemical nature
1.	7.29	Cyclotetrasiloxane, octamethyl-	$C_8H_{24}O_4Si_4$	Siloxane
2.	9.85	Cyclopentasiloxane, decamethyl-	$C_{10}H_{30}O_5Si_5$	Siloxane
3.	12.39	Cyclohexasiloxane, dodecamethyl-	$C_{12}H_{36}O_6Si_6$	Siloxane
4.	14.66	Cycloheptasiloxane, tetradecamethyl-	$C_{14}H_{42}O_7Si_7$	Siloxane
5.	16.68	Cyclooctasiloxane, hexadecamethyl-	$C_{16}H_{48}O_8Si_8$	Siloxane
6.	18.42 22.71	Cyclononasiloxane, octadecamethyl-	$C_{18}H_{54}O_9Si_9$	Siloxane
7.	19.19	Dibutyl phthalate	$C_{16}H_{22}O_4$	Ester
8.	19.98 21.42 23.91 25.16 28.60	Cyclodecasiloxane, eicosamethyl-	$C_{20}H_{60}O_{10}Si_{10}$	Siloxane
9.	24.36	Phthalic acid, di(2-propylpentyl) ester	$C_{24}H_{38}O_4$	Ester
10.	25.77	Pentacyclo[19.3.1.1 (3,7).19,13).1(15,19)] octacosa-1(25),3,5,7 (28),9,11,13(27),15, 17,19 (26),21,23-dodecaene-25,26,27,28-tetrol, 5,11,17,23-tetrakis(1,1-dimethylethyl)	$C_{44}H_{56}O_4$	Alcohol
11.	26.58	13-Docosenamide, (Z)-	$C_{22}H_{43}NO$	Amide
12	27.23	Lupeol	$C_{30}H_{50}O$	Triterpenoid

(Million's test), amino acids (Ninhydrin test), gums and mucilage (swelling test), flavonoids (Shinoda test) in HSAE was confirmed by PPS [46,47].

2.4. Determination of total phenolic and flavonoid content (TPC and TFC)

TPC was analyzed using Folin-Ciocalteu method [48] by mixing the dried HSAE in methanol (1.0 mg/mL). One hundred (100) μL of HSAE in methanol, 125 μL of Folin-Ciocalteu reagent and 750 μL of sodium carbonate solution (15% w/v) were taken in a test tube and the final volume was adjusted to 5.0 mL with deionized water and mixed properly. Absorbance of the above mixture was measured at 760 nm using a spectrophotometer after incubating for 90 min in dark at room temperature. TPC of the samples as milligrams of gallic acid equivalents per gram of dry weight (mg of GAE/g of DW) was determined from a standard curve of gallic acid. All measurements were carried out in triplicate.

Aluminium chloride colorimetric assay was adapted for determining TFC [48]. Briefly, 0.5 mL of HSAE in methanol, 0.1 mL of $AlCl_3$ (10%), 0.1 mL of potassium acetate (1 M) and 1.5 mL of methanol (95%) were taken in a test tube and the volume was adjusted to 5 mL with distilled water and mixed thoroughly. The mixture was incubated for 60 min at room temperature in dark and then the absorbance was measured at 415 nm. TFC was expressed as mg of rutin equivalents per gram dry weight (mg RE/g of DW) of the sample through a standard curve of rutin.

2.5. Gas chromatography mass spectrometry (GC/MS) analysis

One microlitre of HSAE solution in methanol was injected for analysis into GC/MS system consisting of GC (Thermo Tracer 1300) and MS (Thermo TSQ 8000). GC and MS were connected with the following operational conditions: TG 5MS column, electron impact mode at 70 eV, helium as carrier gas with flow rate of 1 mL/min, S/SL injector, 250 °C oven temperature, 280 °C MS transfer line temperature, oven temperature was set at 60 °C and gradually increased (10 °C/min), scan interval of 0.5 s with 50 *m/z* to 700 *m/z* as the complete mass scan range. Xcalibur 2.2 SP1 data acquisition software was employed for data acquisition and interpretation was carried out using NIST software (NIST/EPA/NIH mass spectral library version 2.0 g. NIST 11). The chemical name and nature of the compounds was determined by comparison of the spectrum with the spectrum of the components stored in the NIST library.

2.6. Synthesis of gold nanoparticles (AuNPs)

AuNPs were synthesized by dissolving aqueous tetrachloroaurate-(III) hydrate ($HAuCl_4{\cdot}3H_2O$) (Alfa Aesar, MA, USA) solution (1, 2, 4, 6 and 8 mM) and HSAE (10, 30, 50, 70 and 90% v/v). For synthesis of the NPs, the above reaction mixtures were heated at different temperatures (room temperature, 40, 60, 80 and 100 °C) for varying time duration (15, 30, 45 and 60 min). Optimum pH for synthesis of NPs was also determined by adjusting different pH of reaction mixture (2, 4, 6, 8 and 12) using hydrochloric acid or sodium hydroxide solution. The optimized synthesis reaction for formation of AuNPs was under the following conditions: 10% (v/v) HSAE concentration, 1 mM $HAuCl_4{\cdot}3H_2O$ concentration, 80 °C reaction temperature, pH of 2.0, and 45 min reaction time. The signatory color change because of surface plasmon resonance was monitored visually, confirming the formation of NPs. The reaction mixture was centrifuged at 10,000 rpm (Allegra™ 25R Centrifuge, Beckman Coulter, Inc, Brea, CA, USA) for 10 min to remove any large particles. Then the supernatant was collected and centrifuged again at 14,000 rpm for 1 h. Finally, the AuNP pellet was suspended in distilled water and lyophilized (FreeZone® Plus™, Labconco Corporation, MO, USA) overnight to get the powdered AuNPs [3,25].

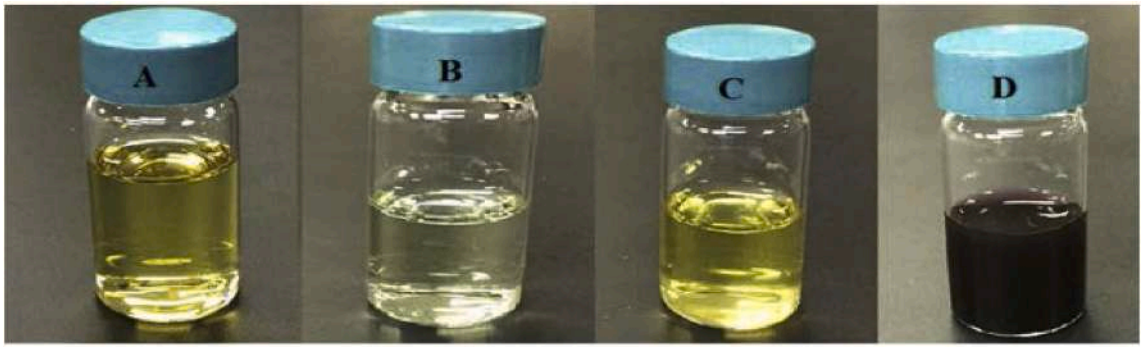

Fig. 2. Color change of reaction mixture during synthesis of AuNPs. **A**: *H. spinosa* aqueous extract (HSAE); **B**, $HAuCl_4$ solution; **C**, reaction mixture immediately after mixing A and B; **D**, color change of reaction mixture after formation of AuNPs under optimum condition (10% HSAE, 1 mM $HAuCl_4$ solution, pH 2.0, 80 °C reaction temperature, and 45 min reaction time). (For interpretation of the references to color in this figure legend, the reader is referred to the Web version of this article.)

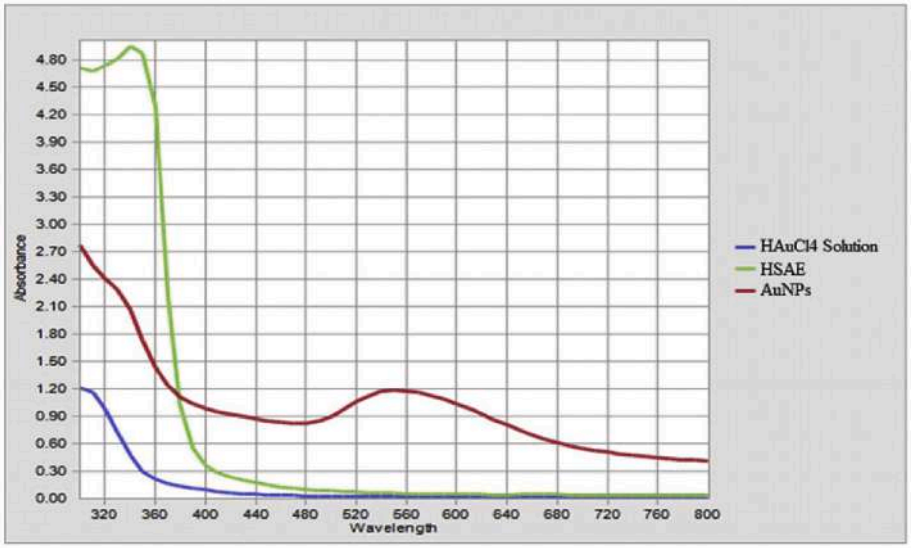

Fig. 3. UV–Vis spectra of *H. spinosa* aqueous extract (HSAE), $HAuCl_4$ solution (1 mM) and synthesized AuNPs under optimum condition.

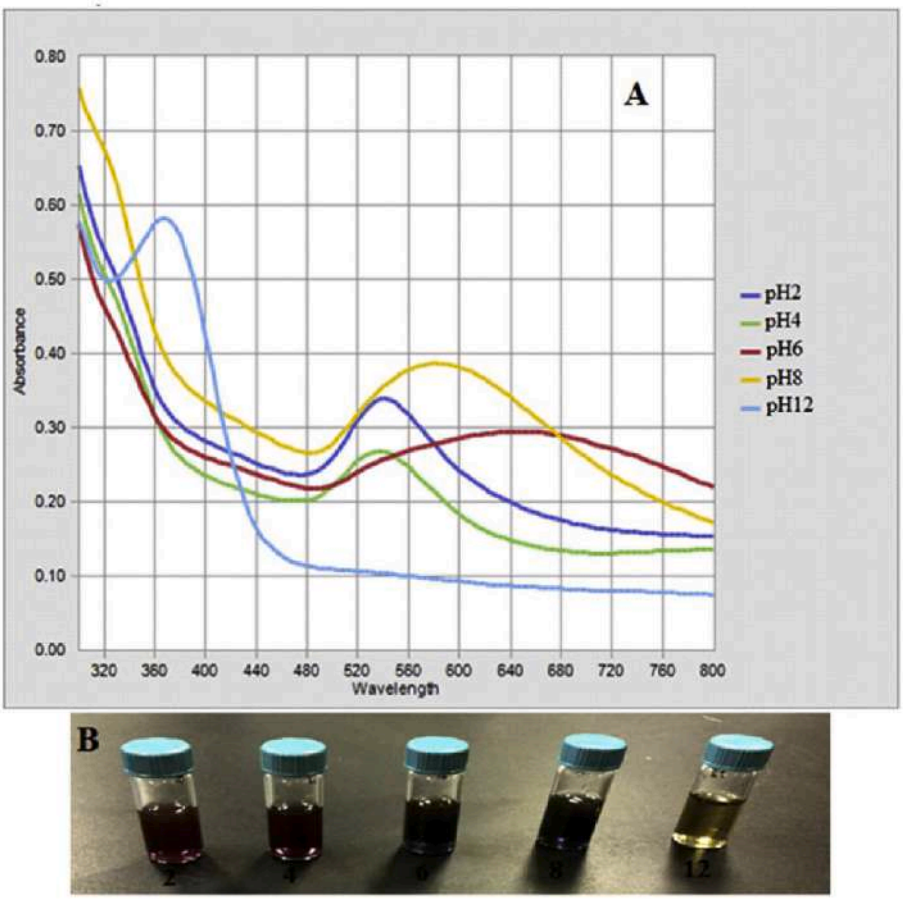

Fig. 4. Effect of pH in synthesis of AuNPs. **(A)** UV–Vis spectra of AuNPs synthesized at different pH values (2, 4, 6, 8 and 12) and **(B)** color change from left to right in various pH values (2, 4, 6, 8 and 12) with 10% of *H. spinosa* extract, 1 mM $HAuCl_4$ solution, at 80 °C for 45 min. (For interpretation of the references to color in this figure legend, the reader is referred to the Web version of this article.)

2.7. Characterization of AuNPs

Characterization of AuNPs was carried out by UV–vis spectroscopy (Varioskan Flash, Thermo Scientific, USA), Particle Size/Zeta Potential analyzer (NanoBrook 90 Plus PALS, Brookhaven Instruments, Holtsville, NY), X-ray diffraction (PANalytical X'Pert MPD diffractometer, PANalytical Inc., Westborough, MA, USA), transmission electron microscopy (TEM, JEOL USA, Inc., Peabody, MA), field emission gun scanning electron microscope (FEG-SEM, Carl Zeiss Microscopy, Thornwood, NY), energy dispersive spectroscopy (EDS, Ametek-EDAX Mahwah, New

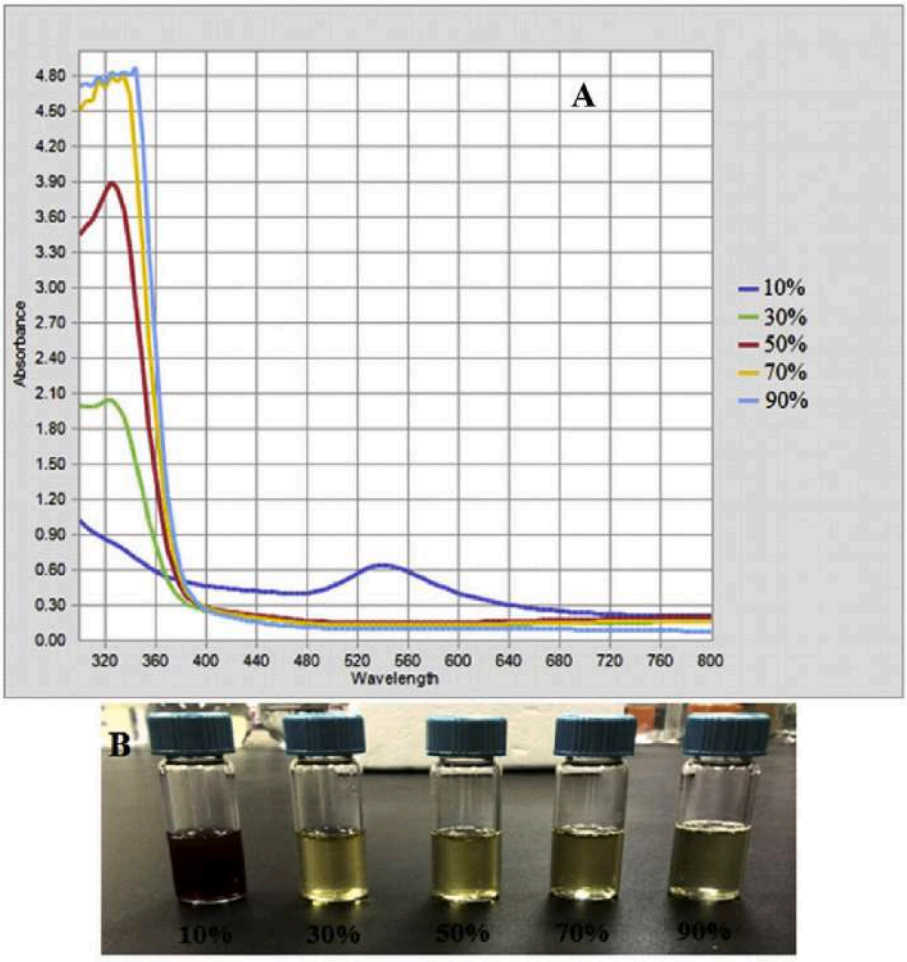

Fig. 5. Effect of plant extract concentration in synthesis of AuNPs. **(A)** UV–Vis spectra of AuNPs synthesized at different concentrations of HSAE (10, 30, 50, 70 and 90% v/v) and **(B)** color change from left to right at different concentrations of HSAE (10, 30, 50, 70 and 90% v/v) with 1 mM $HAuCl_4$ concentration, pH 2, at 80 °C for 45 min. (For interpretation of the references to color in this figure legend, the reader is referred to the Web version of this article.)

Jersey), and fourier transform infrared spectroscopy **(**FTIR, Nicolet iS10, Thermo Scientific, USA). Biosynthesis of NPs at different reaction conditions and their stability was analyzed using UV–vis spectrophotometry in the range between 300 and 800 nm. Particle size, size distribution and surface charge (zeta potential) were evaluated using Particle Size/Zeta Potential analyzer. Surface morphology of the synthesized AuNPs was determined by TEM and FEG-SEM. Elemental composition of AuNPs was analyzed by EDS, involvement of various functional groups in NP synthesis was investigated by FTIR and crystalline nature of synthesized NPs was obtained by XRD.

2.8. Determination of total antioxidant capacity (TAC)

TAC of AuNPs and HSAE as μM copper reducing equivalents (CRE) was determined by following the protocol mentioned in the product manual of OxiSelect™ TAC Assay Kit (Cell Biolabs, Inc., San Diego, CA, USA; Catalog Number: STA- 360) [49,50].

2.9. Cell lines and culture

MCF-7 and MDA-MB-231 (breast cancer), SKOV-3 (ovarian cancer), NCI/ADR-RES (multi-drug resistant ovarian cancer) and U-87 (glioblastoma, brain cancer) cell lines were procured from ATCC (Manassas, VA). DMEM (Mediatech, Manassas, VA) media was used for culture of breast, ovarian and brain cancer cells, while RPMI 1640 media was used for NCI/ADR-RES cells. Both the media were supplemented with 10% fetal bovine serum (Mediatech, Manassas, VA) and 1% penicillin/streptomycin (Mediatech, Manassas, VA). Cells were maintained in a humidified environment of 5% carbon dioxide at 37 °C.

2.10. In vitro cytotoxicity study

All cancer cell lines (3000, 3000, 4000 and 2000 cells/well of breast, ovarian, multi-drug resistant and brain cancer cell lines, respectively) were seeded in 96-well tissue culture plates. The cells were allowed to grow and attach in the 96-well plate for 24 h. After 24 h, the medium was reinstated with fresh medium containing HSAE or AuNPs at different concentrations (12.5–200 μg/mL). Control wells were also maintained without addition of any drug/preparation and the cells were incubated at 37 °C and 5% CO_2 for 72 h. The media was then taken out and 50 μL of MTT [3-(4,5-dimethylthiazol-2-yl)-2,5-diphenyltetrazolium bromide] solution (0.5 mg/mL) in media was added to each well after washing the cells with sterile PBS. Further, the cells were incubated in similar condition for another 4 h. Finally, the media was removed and hundred microlitre of dimethylsulfoxide (DMSO) was added to each well which dissolves the formazan crystal formed from MTT. Cell viability was assessed by measuring absorbance at 570 nm on a micro plate reader (Varioskan Flash, Thermo Scientific, USA) and percentage cell viability in each treatment was calculated from the following formula.

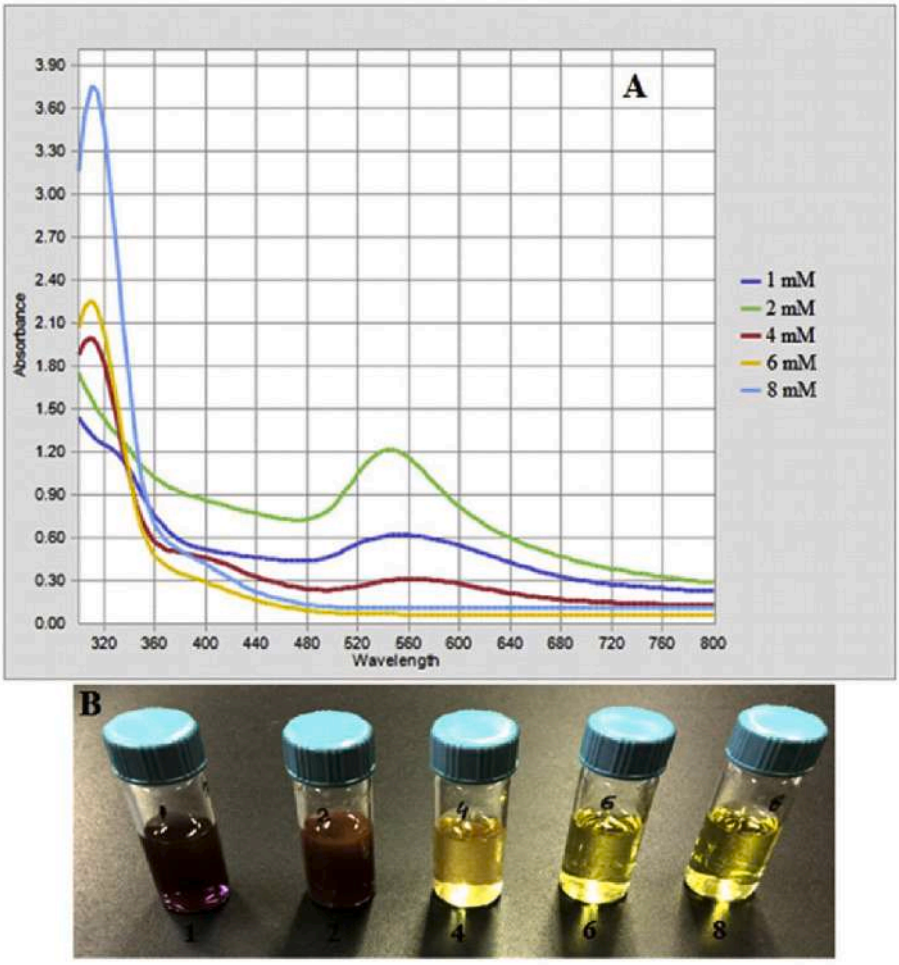

Fig. 6. Effect of $HAuCl_4$ concentration in synthesis of AuNPs. **(A)** UV–Vis spectra of AuNPs synthesized at different concentrations of $HAuCl_4$ (1, 2, 4, 6 and 8 mM) and **(B)** color change from left to right at different concentrations of $HAuCl_4$ (1, 2, 4, 6 and 8 mM) with 10% of HSAE, pH 2, at 80 °C for 45 min. (For interpretation of the references to color in this figure legend, the reader is referred to the Web version of this article.)

$$\%\ \text{Cell Viability} = \frac{Absorbance\ of\ test}{Absorbance\ of\ control} X\ 100$$

2.11. Statistical analysis

For antioxidant and anticancer activities, data were represented as mean ± standard error of mean (SEM). Microsoft Excel was used to access statistical significance ($p < 0.05$) by Student's two-tailed unpaired *t*-test.

3. Results and discussion

3.1. Phytochemical analysis

In the synthesis of metal NPs, various plant secondary metabolites which could cause reduction of metal salt, and work as capping and stabilizing agents are phenolics, flavonoids, alkaloids, polysaccharides, terpenoids along with amino acids, vitamins, proteins and organic acids [51–53]. HSAE was found to contain different plant metabolites such as carbohydrates, flavonoids, gums and mucilage, proteins, amino acids, and tannins and phenolic compounds (Table 1) which might have significant role in synthesis of gold NPs by reduction of the metal salt [3]. Further, the total phenolic content (TPC) and total flavonoid content (TFC) of HSAE was 21.33 ± 2.37 mg GAE/g DW and 33.22 ± 3.39 mg RE/g DW. Phenolics and flavonoids are well known as anticancer and apoptosis inducing agents [54]. In addition, these are also powerful antioxidants and free radical scavengers [55].

3.2. GC/MS analysis of HSAE

Twelve different chemical constituents were identified in HSAE (Fig. 1; Table 2), which were of different chemical nature (alcohols, amides, triterpenoids, esters, siloxane derivatives). The siloxane derivatives are probably due to bleeding of the capillary column and dibutyl phthalate may be a contamination from glassware. Lupeol (a phytosterol and triterpene) found in the extract may be contributing for biosynthesis of NPs and anticancer activity [56,57].

3.3. Biosynthesis of AuNPs and optimization of different reaction parameters

The formation of AuNPs was observed visually through color change to ruby red (Fig. 2) due to surface plasmon resonance (SPR). Fig. 3 indicated that no peak was observed at wavelength of 540 nm for $HAuCl_4$ solution and HSAE. However, the characteristic surface plasmon resonance (SPR) peak was observed after the formation of AuNPs (Fig. 3). Similar characteristic peak at 540 nm was also reported in earlier studies for biosynthesis of AuNP with other plant extracts [58,59]. The position of the SPR peak varies around 540 nm in the visible spectrum of light depending on the shape and size of the nanoparticles [3,5,25,59,60]. Previous studies [60–62] reported the SPR peaks only in the visible spectrum but have not reported any absorption peak in the

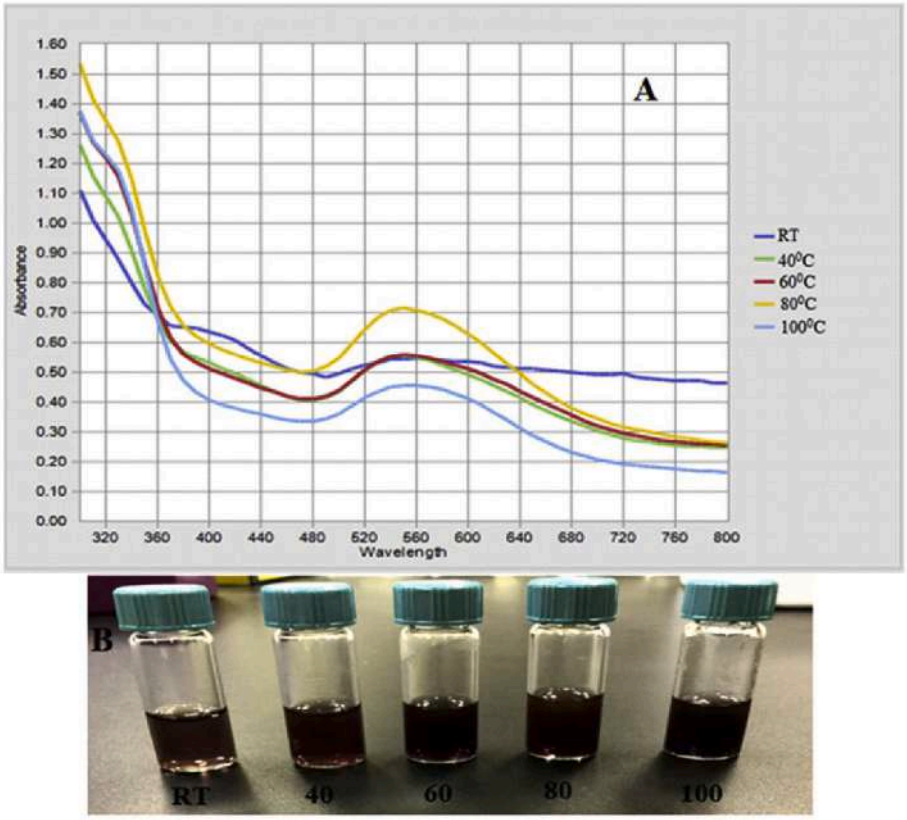

Fig. 7. Effect of reaction temperature in synthesis of AuNPs. **(A)** UV–Vis spectra of AuNPs synthesized at different reaction temperature (room temperature, 40, 60, 80 and 100 °C) and **(B)** color change from left to right at different reaction temperature (room temperature, 40, 60, 80 and 100 °C) with 10% HSAE, 1 mM $HAuCl_4$ solution, pH of 2 for 45 min. (For interpretation of the references to color in this figure legend, the reader is referred to the Web version of this article.)

320–340 nm. In this study, we are reporting the absorption spectrum from 300 to 800 nm. The peak in 320–360 nm region may be due to some of the phytoconstituents in the HSAE (Fig. 3).

The initial pH of metal salt solution plays significant role in formation of AuNPs. In case of AuNP synthesis the characteristic SPR peak was obtained at pH 2 of $HAuCl_4$ solution with other parameters as 10% of HSAE, 1 mM $HAuCl_4$ solution, 80 °C reaction temperature and 45 min reaction time. At pH 6.0 and 8.0 the absorption peak shifted towards right. An increase in pH may have caused degradation of the NPs as indicated from the color of the reaction mixture (see Fig. 4A and B). Shifting of peak towards higher wavelength and broadening of peaks at pH 6 and 8 might be due to secondary reduction of gold ions or formation of larger nanoparticles [61]. The characteristic SPR peak at 540 nm could not be found at pH 12.0, but at this pH an intense band around 370 nm was observed. The peak around ~370 nm at pH 12 may be due to AuNPs of different size and morphology, or degradation products from HSAE. The color of the reaction mixture changed to ruby red within 5 min at pH 6, 8 and 12, but the final colors after 45 min were deep blue (pH 6 and 8) and light greenish (pH 12). The color change indicates that the reaction mixtures were unstable under these conditions and may have formed different size and type of NPs. The reaction rate was faster with weak acidic (pH 6) and alkaline (pH 8 and 12) treatment compared to acidic (pH 2 and 4) treatment. The peak at pH 6 & 8 are broader indicating the presence of different sizes and morphologies of AuNPs [61]. In case of pH 2 & 4 the bands were narrow. The maximum SPR peak intensity was observed at pH 2 indicating presence of AuNPs of smaller size and spherical shape. Further, the peak at pH 2 was highly symmetrical, which may be due to uniform distribution of the AuNPs. Our observation of broadening of peak at higher pH and stability of synthesized AuNPs at lower pH agree with the earlier reports [25,63]. From the observations, pH 2 was selected as optimum pH for further synthesis of AuNPs.

The characteristic SPR peak (520–560 nm range) and desired color change (ruby red) in synthesis of AuNPs was obtained only with 10% of HSAE (see Fig. 5A and B). The results indicate that the extract contains enough reducing agents and 10% HSAE is required for biosynthesis of AuNPs. Excess amount of some phytochemicals and protons in HSAE (30, 50, 70 and 90%) may have affected the nucleation of AuNPs or kept the chloroauric acid in molecular form preventing the reduction of Au (III) to Au(0) as shown below [61].

$$HAuCl4 \rightarrow AuCl^{-}4 + H^{+} \quad (1)$$

$$AuCl^{-}4 \rightarrow AuCl \rightarrow Au(0) \quad (2)$$

Previous studies with other plant extracts demonstrated a wide range of concentrations (7–70%) of plant extracts in synthesis of AuNPs [3,5,9,17,25]. The peak(s) around ~330 nm with HSAE (30, 50, 70 and 90%) may be due to different sized NPs or the degraded products of NPs or degradation products from HSAE. The intensity of the peak(s) increases with higher concentration of HSAE.

Fig. 6A and B shows the effect of different concentrations of chloroauric acid ($HAuCl_4$) on synthesis of NPs. NPs were synthesized with 10% of HSAE, pH 2, at 80 °C reaction temperature for 45 min. Characteristic SPR peak (520–560 nm range) was observed with 1–4 mM $HAuCl_4$ concentrations. The NPs were agglomerated with increase in particle size (more than 1000 nm) with 2 mM $HAuCl_4$ concentration. The appearance of the suspension with 2 mM $HAuCl_4$ concentration indicated particle precipitation or aggregation, and instability. The intensity of the SPR peak at ~540 decreased with $HAuCl_4$ concentration more than 2 mM. The excessive Au(III) ions in the reaction mixture may have exhausted most of the reducing agents in HSAE and the remaining phytoconstituents were not adequate to work as reducing and stabilizing

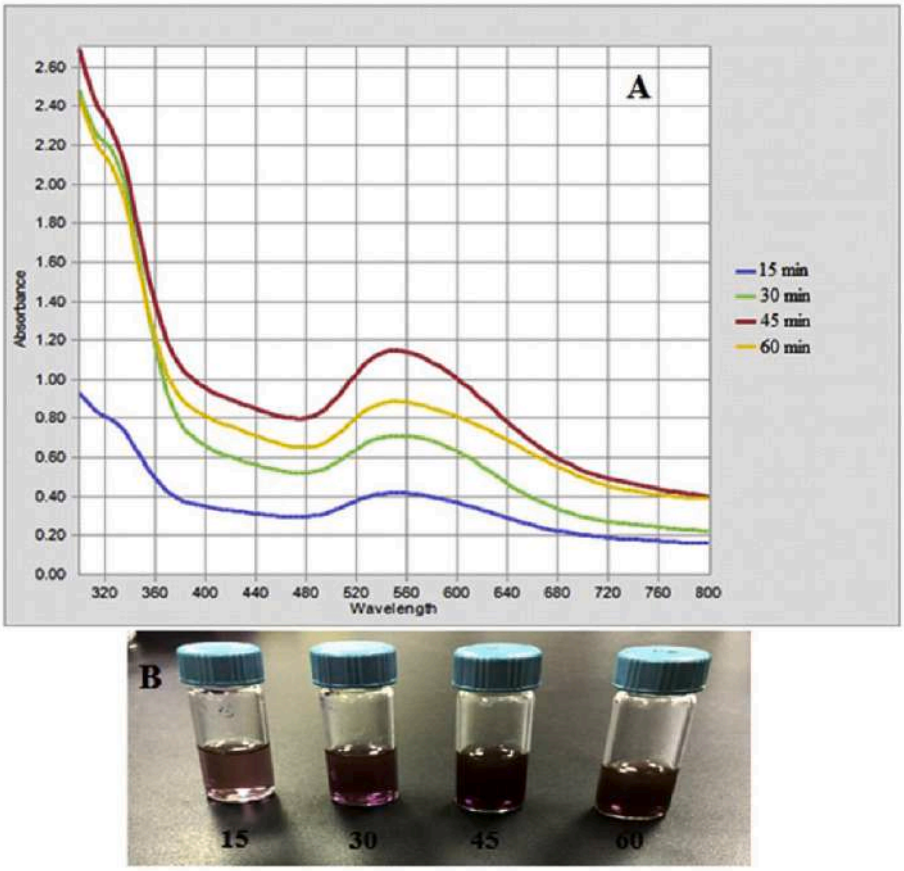

Fig. 8. Effect of reaction time in synthesis of AuNPs. **(A)** UV–Vis spectra of AuNPs synthesized at different reaction times (15, 30, 45 and 60 min) and **(B)** color change from left to right after reaction for different reaction times (15, 30, 45 and 60 min) with 10% HSAE, 1 mM $HAuCl_4$ solution, pH of 2 at 80 °C. (For interpretation of the references to color in this figure legend, the reader is referred to the Web version of this article.)

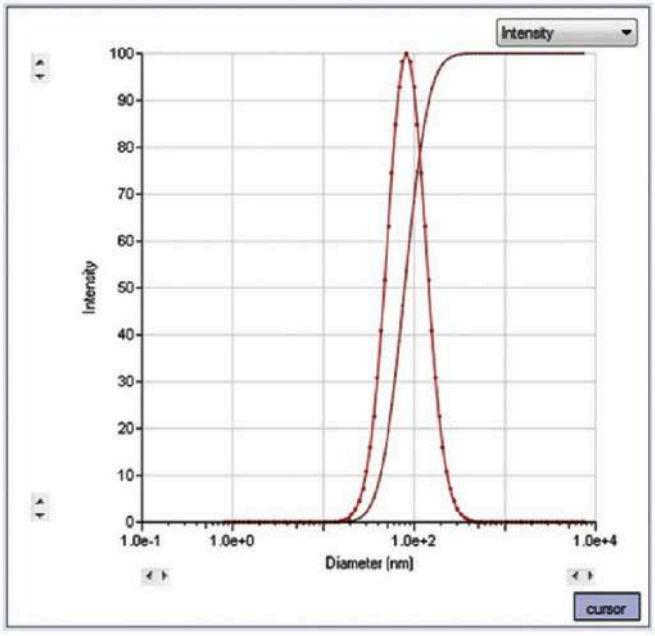

Fig. 9. Particle size of AuNPs synthesized with HSAE (10% HSAE, 1 mM $HAuCl_4$ solution, pH of 2, and 45 min reaction time at 80 °C).

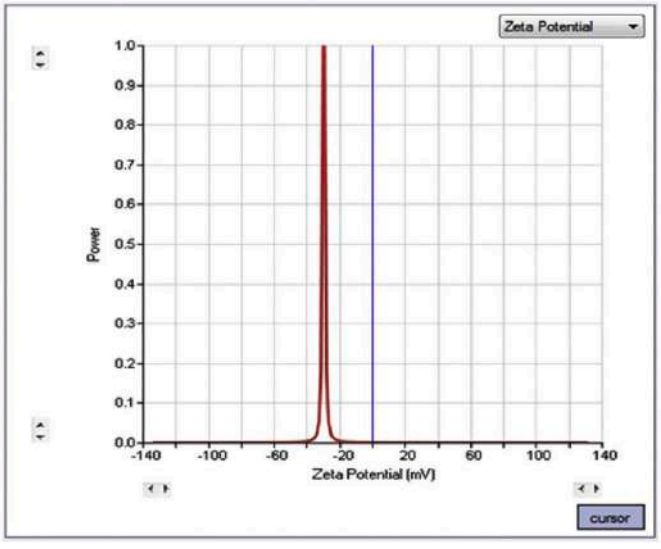

Fig. 10. Zeta potential of AuNPs synthesized with HSAE (10% HSAE, 1 mM $HAuCl_4$ solution, pH of 2, and 45 min reaction time at 80 °C).

agents for formation of AuNPs. Broader peak at 500–640 nm range with 4 mM $HAuCl_4$ concentration indicated that the synthesized AuNPs had different morphology and larger size. Formation of AuNP in lower salt concentration and broadening of peaks in higher concentration was also reported by Markus et al. [25]. At higher concentrations of $HAuCl_4$, the

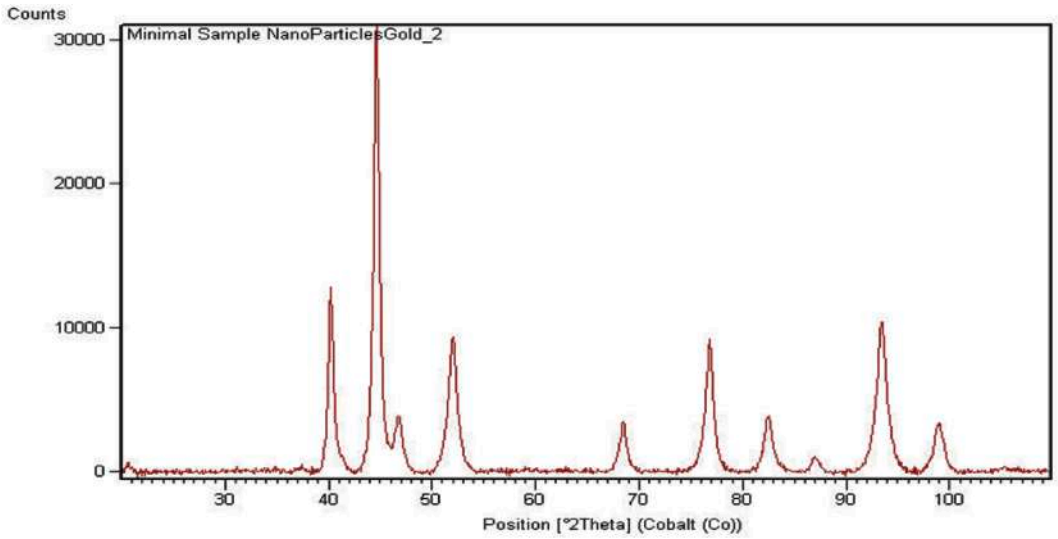

Fig. 11. XRD pattern of AuNPs synthesized using HSAE (10% HSAE, 1 mM $HAuCl_4$ solution, pH of 2, and 45 min reaction time at 80 °C).

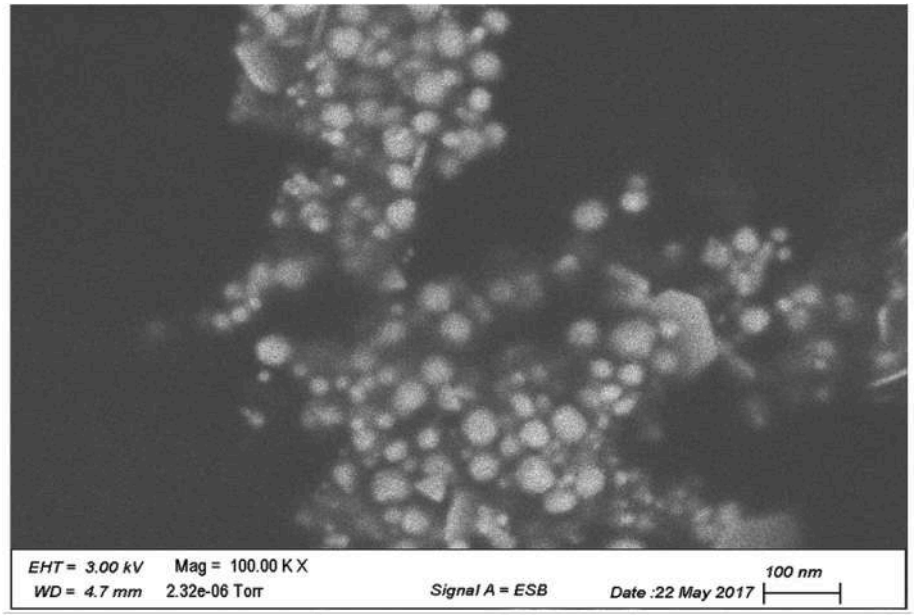

Fig. 12. SEM images of AuNPs synthesized using HSAE (10% HSAE, 1 mM $HAuCl_4$ solution, pH of 2, and 45 min reaction time at 80 °C).

intensity of the peak at around 320 nm increased. The peak around 320 nm with higher concentration of $HAuCl_4$ may be due to formation of different size and morphology of AuNPs, or degradation products from HSAE. For further synthesis of AuNPs, 1 mM $HAuCl_4$ concentration was selected as the optimum salt concentration.

Biosynthesis of AuNPs was also performed at different temperature (room temperature, 40, 60, 80 and 100 °C) with 10% (v/v) HSAE, 1 mM $HAuCl_4$ concentration, pH 2 and reaction time for 45 min. At room temperature, the characteristic SPR peak was too broad confirming the large size of synthesized AuNPs. The maximum peak intensity was observed at 80 °C with smaller particle size and uniform distribution of the NPs. The absorption peaks were broadened and lowered at 40, 60 and 100 °C demonstrating incomplete formation of AuNPs at lower temperature and aggregation of the AuNPs at temperature above 80 °C. Further, degradation of the plant secondary metabolites at higher temperature also broadens the absorption peak [25]. Fig. 7A and B shows the absorption peaks and color change of reaction mixture at different reaction temperatures.

Fig. 8A, B shows the effect of duration of reaction time on the formation of AuNPs [at 10% (v/v) HSAE, 1 mM $HAuCl_4$ solution, pH 2 and reaction temperature 80 °C]. Highest absorbance and symmetrical SPR peak at around 540 nm were observed at 45 min of reaction time. This confirms the smaller and uniform sizes of the AuNPs. With increase in the reaction time, the peak intensity of AuNPs decreased. The absorption peak with 60 min reaction time was broader indicating the existence of larger and higher polydisperse sizes of the NPs. The ruby red color intensity increased up to 45 min of reaction time and at 60 min, the presence of particulate matters was observed. The size of the AuNPs was more than 600 nm and the polydispersity index were around 0.8 with the 60 min of reaction time.

3.3.1. *Stability of biosynthesized nanoparticles*

The stability of the freshly biosynthesized AuNPs at room temperature was confirmed by UV–Vis analysis over a period of 10 days. Similar absorption spectrum was demonstrated by the reaction mixture at various time intervals. Further, there was no significant alteration of

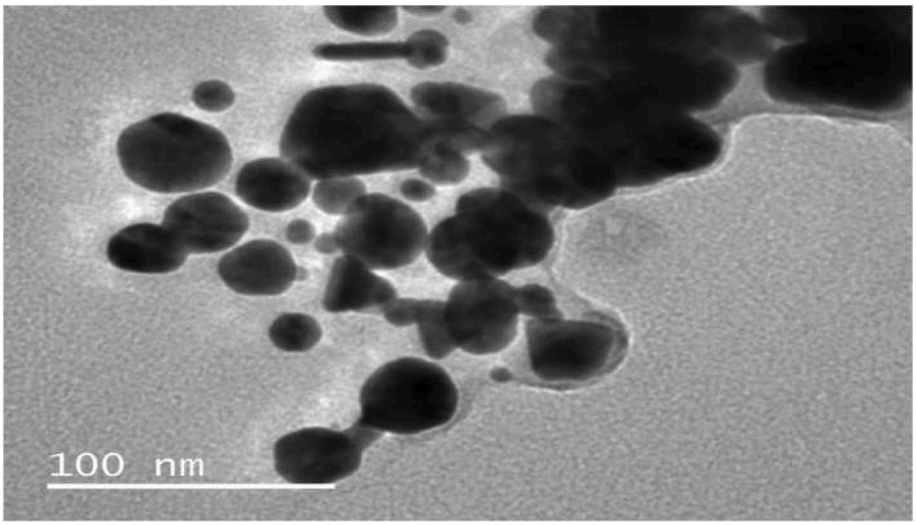

Fig. 13. TEM images of AuNPs synthesized using HSAE (10% HSAE, 1 mM $HAuCl_4$ solution, pH of 2, and 45 min reaction time at 80 °C).

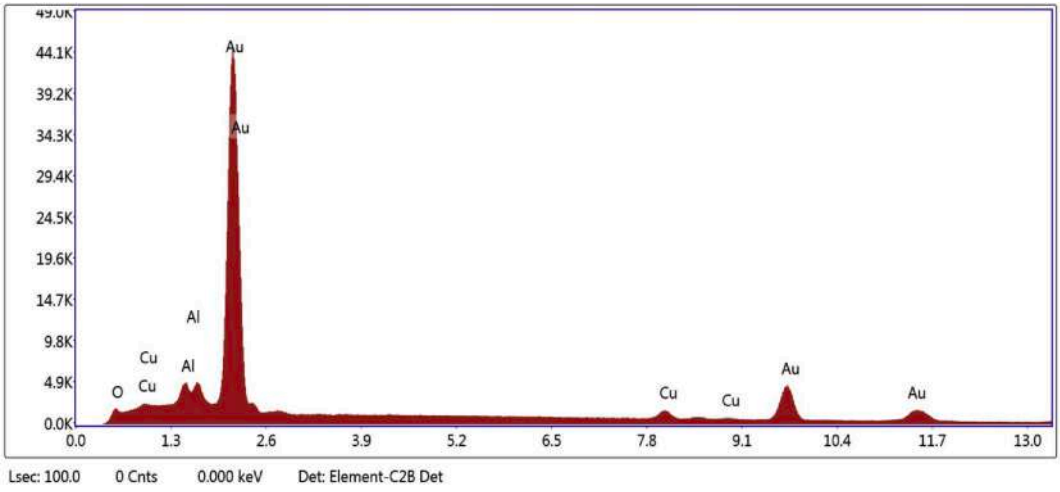

Fig. 14. EDS spectrum of AuNPs synthesized using HSAE (10% HSAE, 1 mM $HAuCl_4$ solution, pH of 2, and 45 min reaction time at 80 °C).

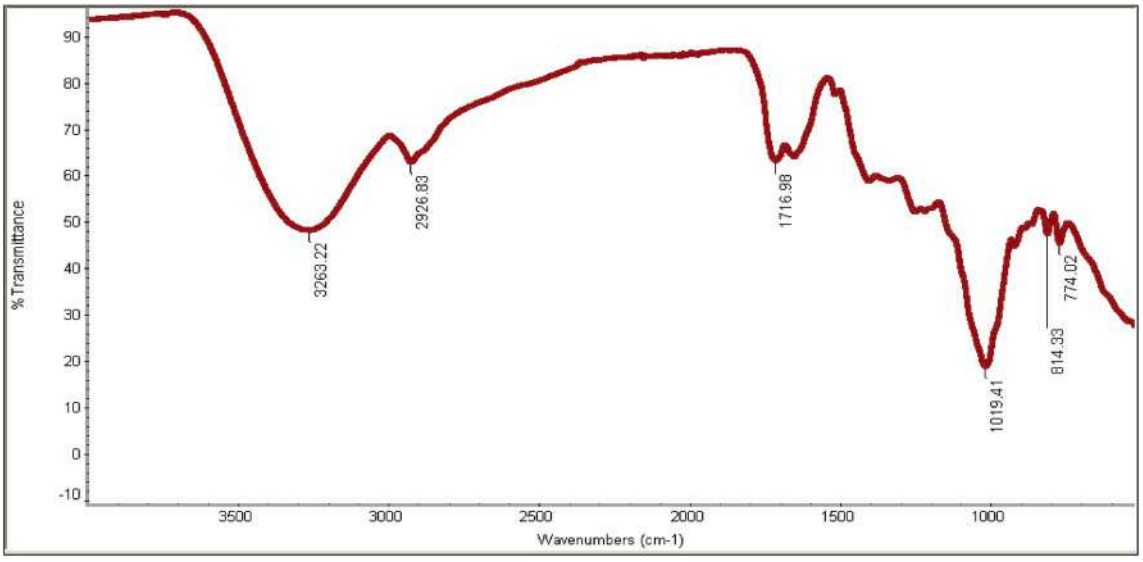

Fig. 15. FTIR spectrum of AuNPs synthesized using HSAE (10% HSAE, 1 mM $HAuCl_4$ solution, pH of 2, and 45 min reaction time at 80 °C).

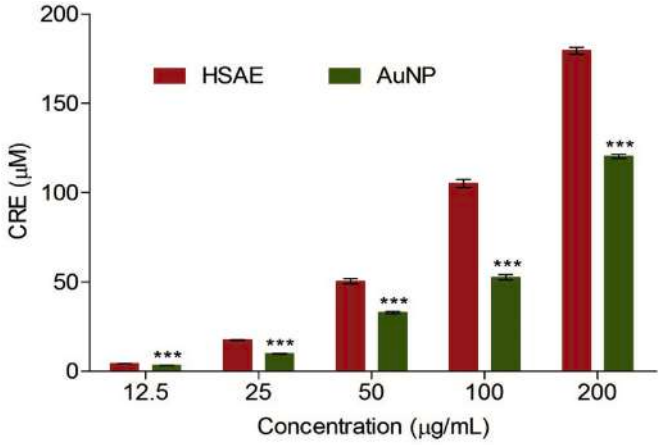

Fig. 16. Total antioxidant capacity of *H. spinosa* aqueous extract (HSEA) and synthesized AuNPs (10% HSAE, 1 mM $HAuCl_4$ solution, pH of 2, 45 min reaction time at 80 °C). Values are mean ± SEM (n = 3); ***p < 0.001 vs HSAE at the same dose, AuNP, gold nanoparticles synthesized with HSEA; CRE, copper reducing equivalent. (For interpretation of the references to color in this figure legend, the reader is referred to the Web version of this article.)

particle size signifying the stability of the synthesized AuNPs.

3.4. Particle size and zeta potential

The particle size and polydispersity index (PDI) of biosynthesized AuNPs at optimized condition (10% HSAE, 1 mM $HAuCl_4$ solution, pH of 2, 45 min reaction time at 80 °C) were 68.44 ± 0.30 nm and 0.283 ± 0.012, respectively (Fig. 9). Particle size (by DLS analysis) in this study was smaller compared to gold nanoparticles synthesized with extracts of *Musa paradisiacal* [3], ginseng [5,58] and *Angelica pubescens* [25]. The PDI of AuNPs was found to be moderate. Various plant metabolites of HSAE (sugars, phenolics, flavonoids and proteins) may probably protect the agglomeration of AuNPs by forming capping layer around the synthesized AuNPs [64]. Zeta potential of the biosynthesized AuNPs was found to −27.78 ± 0.66 mV (Fig. 10). Zeta potential is a determinant of the stability of the NPs and high surface charge prevents aggregation of NPs by electrostatic repulsion between the NPs [65].

3.5. XRD analysis

Crystalline structure and phase identification of the synthesized AuNPs was confirmed by XRD analysis. XRD analysis of AuNPs showed several diffraction peaks. The four peaks at 40.25, 44.65, 68.45 and 76.85 (Fig. 11) confirm the crystalline nature of the AuNPs and are characteristic diffraction peaks for face center cubic (FCC) structure of the AuNPs [3,25].

3.6. TEM and SEM analyses

Surface morphology of NPs in nanometer to micrometer range could be determined by SEM and TEM analysis [6]. TEM and SEM analysis of AuNPs showed spherical, polygonal, rod and triangular shaped particles (Figs. 12 and 13). Various shaped NPs are commonly formed in the same batch during green synthesis of gold nanoparticles [3,66,67]. The size variation of NPs could be due to the presence of different secondary metabolites (reducing agent) in HSAE [68]. The particle size of AuNPs by DLS method was slightly larger compared to TEM and SEM analysis. Similar results were also reported in earlier studies [5,25].

3.7. Energy dispersive spectroscopy

Presence of different elements and their proportion in a sample is

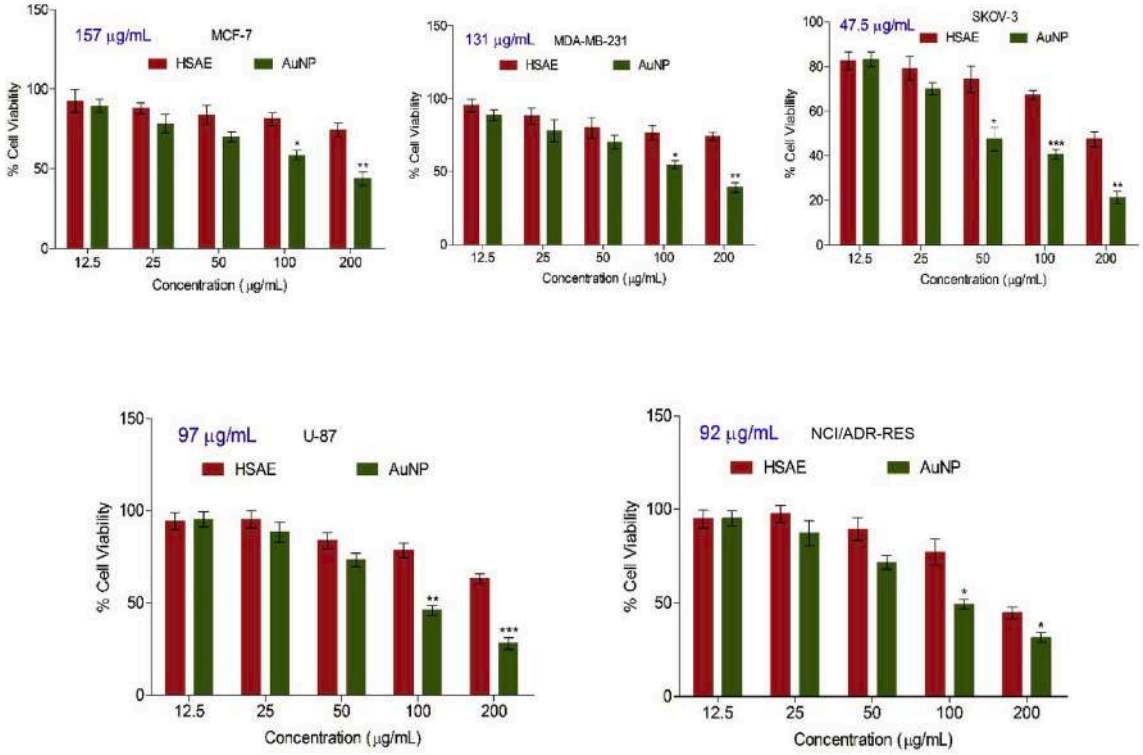

Fig. 17. In vitro cytotoxicity of *H. spinosa* aqueous extract (HSEA) and synthesized AuNPs in MCF-7, MDA-MB-231, SKOV-3, U-87 and NCI/ADR-RES cells after 72 h of incubation by MTT assay. Values are mean ± SEM (n = 3); *p < 0.01, **p < 0.01, ***P < 0.001 versus HSEA treatment at the same concentration; AuNP, gold nanoparticles synthesized with HSEA; Digits in blue color indicates the IC50 value of AuNP against the respective cancer cell line. (For interpretation of the references to color in this figure legend, the reader is referred to the Web version of this article.)

confirmed by EDS analysis [2,5]. The EDS spectrum of the AuNPs showed the presence strong signals of Au with some other signals of O, Cu, and Al (Fig. 14).

3.8. Fourier transform infrared spectroscopy

FTIR was performed for ascertaining the probable biomolecules responsible for formation of metal NPs by reduction of the metal ions. FTIR spectrum of biosynthesized AuNPs showed peaks at 3263.22, 2926.83, 1716.98, 1019.41, 814.33 and 774.02 (Fig. 15). Peak at 3263.22 may be assigned to O–H stretching of phenolic and/or alcoholic groups and suggests the involvement of flavonoids, tannins and phenolic compounds in reducing the metal ions. Peak at 2926.83 corresponds to C–H stretching of methylene, methyl, and methoxy groups. The peak at 1716.98 represents C═O stretching of fatty acids, esters and ketones. The intense band at 1019.41 corresponds to the (C–O) bond stretching of ester, carbohydrate and Si–O–Si asymmetric stretching of siloxanes. Absorption peaks at 814.33 and 774.02 are affiliated to stretching of glycosidic linkage in carbohydrates.

The different classes of chemical compounds confirmed by preliminary phytochemical screening in HSAE were carbohydrates, tannins and phenolics, proteins, amino acids, gums and mucilage, flavonoids and organic acids. HSAE demonstrated alcohols, amides, triterpenoids and esters by GC/MS analysis. The results corroborate the stabilization of biosynthesized metal NPs by the free functional groups of different chemical constituents present in the extract [3,25].

3.9. Antioxidant activity

Total antioxidant capacity (TAC) of both HSAE and AuNPs was determined and represented as copper reducing equivalent (CRE) (Fig. 16). AuNPs exhibited dose dependent antioxidant activity, but the potency is less than the extract. Determination of TAC is frequently used to evaluate the antioxidant response of biological samples against free radicals generated during various disease conditions [69]. Antioxidant status of a sample is directly proportional to its TAC. The findings suggest that the antioxidant activity of biosynthesized AuNPs could be attributed to the secondary metabolites (phenolic compounds) of the extract which forms the capping layer [25]. Many nanoparticles induce production of reactive oxygen species (ROS) and may cause cell death [70,71]. These side effect or toxicity due to ROS could be ameliorated by antioxidants. In addition, antioxidants play major role in management of various diseases including cancer [72,73]. The green synthesized AuNPs in the present study with antioxidant property could be a better option for prevention of diseases.

3.10. In vitro anticancer activity

In vitro cytotoxicity of the synthesized AuNPs and HSAE against MCF-7 and MDA-MB-231 (breast), SKOV-3 (ovarian), NCI/ADR-RES (multi-drug resistant ovarian) and U-87 (brain) cancer cell lines was determined at concentrations ranging from 12.5 to 200 μg/mL by MTT assay (Fig. 17). AuNPs exhibited dose dependent cytotoxicity against all the cancer cell lines. The percentage cell viability by synthesized AuNPs at 200 μg/mL against MCF-7, MDA-MB-231, SKOV-3, NCI/ADR-RES and U-87 cell lines was 43.78, 39.34, 21.45, 31.48 and 27.89%, respectively. Synthesized AuNPs showed more cytotoxicity in ovarian cancer cell line than breast, brain and multi-drug resistant ovarian cancer cell lines. Biosynthesized AuNPs demonstrated significantly higher anticancer activities compared to HSAE which may be attributed to increased cellular uptake and retention of the NPs. In addition, the NPs are not substrates for the P-glycoprotein efflux pump [74].

4. Conclusion

H. spinosa aqueous extract (HSAE) has been used for green synthesis of gold nanoparticles (AuNPs). Visual color change and UV–Vis analysis corroborated that 10% HSAE, 1 mM $HAuCl_4$ solution, pH of 2, 80 °C reaction temperature and 45 min reaction time were the optimized conditions for AuNP synthesis. The AuNPs have small particle size (68.44 ± 0.30 nm) and zeta potential of −27.78 mV. Phytochemical screening and GC/MS analysis showed the different secondary metabolites (proteins, flavonoids, phenolics, carbohydrates and terpenoids) that helped for reduction and capping process in the synthesis of AuNPs. FTIR spectrum of biosynthesized AuNPs indicated the involvement of different functional groups during the formation of AuNPs. AuNPs at higher concentrations (100 and 200 μg/mL) exhibited significantly enhanced *in vitro* cytotoxicity against various tested cancer cell lines (breast, ovarian, multi-drug resistant ovarian and brain) than HSAE. The green synthesized AuNPs with combined antioxidant and cytotoxicity properties could be a better approach for nanomedicine. The AuNPs synthesized in this eco-friendly manner could be further investigated as theranostic (therapeutic and diagnostic) tool for treatment of cancer.

Declaration of competing interest

None.

Acknowledgements

Financial support of University Grants Commission, New Delhi, India to AP as Raman Fellowship for Postdoctoral Research in USA is greatly acknowledged. The authors are thankful to Dr. Pankaj Samuel, Application Scientist, GC/MS laboratory, Panjab University, Chandigarh, India for GC/MS analysis and Mr. Michael Dunlap, University of California, Merced, USA for SEM, TEM, EDS and XRD studies.

References

[1] P.K. Jain, K.S. Lee, I.H. El-Sayed, M.A. El-Sayed, Calculated absorption and scattering properties of gold nanoparticles of different size, shape, and composition: applications in biological imaging and biomedicine, J. Phys. Chem. B 110 (2006) 7238–7248.

[2] K. Venugopal, H.A. Rather, K. Rajagopal, M.P. Shanthi, K. Sheriff, M. Illiyas, R. A. Rather, E. Manikandan, S. Uvarajan, M. Bhaskar, M. Maaza, Synthesis of silver nanoparticles (Ag NPs) for anticancer activities (MCF 7 breast and A549 lung cell lines) of the crude extract of *Syzygium aromaticum*, J. Photochem. Photobiol. B: Biol. 167 (2017) 282–289.

[3] S. Vijayakumar, B. Vaseeharan, B. Malaikozhundan, N. Gopi, P. Ekambaram, R. Pachaiappan, P. Velusamy, K. Murugan, G. Benelli, R. Suresh Kumar, M. Suriyanarayanamoorthy, Therapeutic effects of gold nanoparticles synthesized using *Musa paradisiaca* peel extract against multiple antibiotic resistant *Enterococcus faecalis* biofilms and human lung cancer cells (A549), Microb. Pathog. 102 (2017) 173–183.

[4] M.C. Daniel, D. Astruc, Gold nanoparticles: assembly, supramolecular chemistry, quantum-size-related properties, and applications toward biology, catalysis, and nanotechnology, Chem. Rev. 104 (2004) 293–346.

[5] P. Singh, Y.J. Kim, C. Wang, R. Mathiyalagan, M.E. Farh, D.C. Yang, Biogenic silver and gold nanoparticles synthesized using red ginseng root extract, and their applications, Artif. Cells Nanomed. Biotechnol. 44 (2016) 811–816.

[6] B. Sadeghi, M. Mohammadzadeh, B. Babakhani, Green synthesis of gold nanoparticles using *Stevia rebaudiana* leaf extracts: characterization and their stability, J. Photochem. Photobiol. B: Biol. 148 (2015) 101–106.

[7] I.H. El-Sayed, X. Huang, M.A. El-Sayed, Surface plasmon resonance scattering and absorption of anti-EGFR antibody conjugated gold nanoparticles in cancer diagnostics: applications in oral cancer, Nano Lett. 5 (2005) 829–834.

[8] M. Rai, A.P. Ingle, S. Birla, A. Yadav, C.A. Santos, Strategic role of selected noble metal nanoparticles in medicine, Crit. Rev. Microbiol. 42 (2016) 696–719.

[9] M. Noruzi, D. Zare, K. Khoshnevisan, D. Davoodi, Rapid green synthesis of gold nanoparticles using *Rosa hybrida* petal extract at room temperature, Spectrochim. Acta Part A Mol. Biomol. Spectrosc. 79 (2011) 1461–1465.

[10] S.S. Shankar, A. Rai, A. Ahmad, M. Sastry, Rapid synthesis of Au, Ag, and bimetallic Au core-Ag shell nanoparticles using neem (*Azadirachta indica*) leaf broth, J. Colloid Interface Sci. 275 (2004) 496–502.

[11] M. Noruzi, Biosynthesis of gold nanoparticles using plant extracts, Bioproc. Biosyst. Eng. 38 (2015) 1–14.

[12] S.H. Ansari, F. Islam, M. Sameem, Influence of nanotechnology on herbal drugs: a review, "J. Adv. Pharm. Technol. Research"" (JAPTR)" 3 (2012) 142–146.

[13] A. Vaseashta, Nanoscale materials, devices, and systems for chem.-bio sensors, photonics, and energy generation and storage, in: A.K. Vaseashta, I.N. Mihailescu, (Eds.), Functionalized Nanoscale Materials, Devices and Systems, Springer, pp. 3-27.

[14] R.A. Sperling, P.R. Gil, F. Zhang, M. Zanella, W.J. Parak, Biological applications of gold nanoparticles, Chem. Soc. Rev. 37 (2008) 1896–1908.

[15] P. Ghosh, G. Han, M. De, C.K. Kim, V.M. Rotello, Gold nanoparticles in delivery applications, Adv. Drug Deliv. Rev. 60 (2008) 1307–1315.

[16] E. Boisselier, D. Astruc, Gold nanoparticles in nanomedicine: preparations, imaging, diagnostics, therapies and toxicity, Chem. Soc. Rev. 38 (2009) 1759–1782.

[17] S. Mukherjee, V. Sushma, S. Patra, A.K. Barui, M.P. Bhadra, B. Sreedhar, C.R. Patra, Green chemistry approach for the synthesis and stabilization of biocompatible gold nanoparticles and their potential applications in cancer therapy, Nanotechnology 23 (2012) 455103, https://doi.org/10.1088/0957-4484/23/45/455103.

[18] S. Patra, S. Mukherjee, A.K. Barui, A. Ganguly, B. Sreedhar, C.R. Patra, Green synthesis, characterization of gold and silver nanoparticles and their potential application for cancer therapeutics, Mater. Sci. Eng. C 53 (2015) 298–309.

[19] P. Kuppusamy, M.M. Yusoff, G.P. Maniam, N. Govindan, Biosynthesis of metallic nanoparticles using plant derivatives and their new avenues in pharmacological applications – an updated report, Saudi Pharmaceut. J. 24 (2016) 473–484.

[20] V. Arya, Living systems: eco-friendly nanofactories, Dig. J. Nanomater. Biostruct. 5 (2010) 9–21.

[21] A.K. Jha, K. Prasad, K. Prasad, A. Kulkarni, Plant system: nature's nanofactory, Colloids Surf. B Biointerfaces 73 (2009) 219–223.

[22] P. Dauthal, M. Mukhopadhyay, Biosynthesis of palladium nanoparticles using *Delonix regia* leaf extract and its catalytic activity for nitro-aromatics hydrogenation, Ind. Eng. Chem. Res. 52 (2013) 18131–18139.

[23] J.Y. Song, H.K. Jang, B.S. Kim, Biological synthesis of gold nanoparticles using *Magnolia kobus* and *Diopyros kaki* leaf extracts, Process Biochem. 44 (2009) 1133–1138.

[24] D. Philip, Rapid green synthesis of spherical gold nanoparticles using *Mangifera indica* leaf, Spectrochim. Acta Part A Mol. Biomol. Spectrosc. 77 (2010) 807–810.

[25] J. Markus, D. Wang, Y.J. Kim, S. Ahn, R. Mathiyalagan, C. Wang, D.C. Yang, Biosynthesis, characterization, and bioactivities evaluation of silver and gold nanoparticles mediated by the roots of Chinese herbal *Angelica pubescens* Maxim, Nanoscale Res. Lett. 12 (2017), https://doi.org/10.1186/s11671-017-1833-2.

[26] R.K. Das, B.B. Borthakur, U. Bora, Green synthesis of gold nanoparticles using ethanolic leaf extract of *Centella asiatica*, Mater. Lett. 64 (2010) 1445–1447.

[27] Anonymous, The Ayurvedic Pharmacopoeia of India, 7-volume Set, Govt. of India, Ministry of Health and Family Welfare, Department of Indian System of Medicine & Homeopathy, 1999.

[28] A. Patra, S. Jha, P.N. Murthy, Phytochemical and pharmacological potential of *Hygrophila spinosa* T. Anders, Pharmacogn. Rev. 3 (2009) 330–341.

[29] P. Shanmugasundaram, S. Venkataraman, Hepatoprotective and antioxidant effects of *Hygrophila auriculata* (K. Schum) Heine acanthaceae root extract, J. Ethnopharmacol. 104 (2006) 124–128.

[30] M.P.N. Sridhar, N. Nandakumar, T. Rengarajan, M.P. Balasubramanian, Amelioration of mercuric chloride induced oxidative stress by *Hygrophila auriculata* (K.Schum) Heine via modulating the oxidant-antioxidant imbalance in rat liver, J. Biochem. Technol. 4 (2013) 622–627.

[31] U.K. Mazumdar, M. Gupta, S. Maiti, D. Mukherjee, Antitumor activity of *Hygrophila spinosa* on Ehrlich ascites carcinoma and sarcoma-180 induced mice, Indian J. Exp. Biol. 35 (1997) 473–477.

[32] S. Ahmed, A. Rahman, M. Mathur, M. Athar, S. Sultana, Anti-tumor promoting activity of *Asteracantha longifolia* against experimental hepatocarcinogenesis in rats, Food Chem. Toxicol. 39 (2001) 19–28.

[33] D.V. Nair, N.B. Shridhar, K. Jayakumar, Evaluation of anticancer activity of *Asteracantha longifolia* in 7,12-Dimethylbenz(a)anthracene-induced mammary gland carcinogenesis in Sprague Dawley rats, IJNPND 5 (2015) 28–33.

[34] M.A. Amin, I.A. Chowdhury, K.M.M. Mahbub, M. Sattar, M. Shahriar, M.R. Kuddus, M.A. Rashid, Anti-inflammatory and analgesic activities of *Asteracantha longifolia* Nees, Bangladesh Pharm. J. 15 (2012) 171–176.

[35] A. Patra, S. Jha, P.N. Murthy, V.D. Aher, P. Chattopadhyay, G. Panigrahi, D. Roy, Anti-inflammatory and antipyretic activities of *Hygrophila spinosa* T. Anders Leaves (Acanthaceae), Trop. J. Pharmaceut. Res. 8 (2009) 133–137.

[36] M.R. Fernando, S.M.D.N. Wickramasinghe, M.I. Thabrew, E.H. Karunanayaka, A preliminary investigation of the possible hypoglycaemic activity of *Asteracantha longifolia*, J. Ethnopharmacol. 27 (1989) 7–14.

[37] V.S. Thorve, A.D. Kshirsagar, N.S. Vyawahare, P.A. Thakurdesai, A.M. Bhandare, H. spinosa T, Anders ameliorates diabetic neuropathy in Wistar albino rats, J. Compl. Integr. Med. 9 (2012) 1–17.

[38] R. Kanhere, A. Anjana, J. Anbu, M. Sumithra, N.K.F.H. Ahamed, Neuroprotective and antioxidant potential of terpenoid fraction from *Hygrophila auriculata* against transient global cerebral ischemia in rats, Pharm. Biol. 51 (2013) 181–189.

[39] K.G. Ingale, P.A. Thakurdesai, N.S. Vyawahare, Protective effect of *Hygrophila spinosa* against cisplatin induced nephrotoxicity in rats, Indian J. Pharmacol. 45 (2013) 232–236.

[40] M.S. Hussain, S. Fareed, M. Ali, Simultaneous HPTLC-UV530 nm analysis and validation of bioactive lupeol and stigmasterol in *Hygrophila auriculata* (K. Schum) Heine, Asian Pac. J. Trop. Biomed. 2 (2012) S612–S617.

[41] M.S. Hussain, S. Fareed, M. Ali, Hyphenated chromatographic analysis of bioactive gallic acid and quercetin in *Hygrophila auriculata* (K. Schum) Heine growing wildly in marshy places in India by validated HPTLC method, Asian Pac, J. Trop. Biomed. 2 (2012) S477–S483.

[42] S. Sunita, S. Abhishek, A comparative evaluation of phytochemical fingerprints of *Asteracantha longifolia* Nees. using HPTLC, Asian J. Plant Sci. 7 (2008) 611–614.

[43] A.K. Maji, S. Pandit, P. Banerji, D. Banerjee, A validated RP-HPLC method for simultaneous determination of betulin, lupeol and stigmasterol in *Asteracantha longifolia* Nees, Int. J. Pharm. Pharmaceut. Sci. 6 (2014) 691–695.

[44] P. Balraj, S. Nagarajan, Apigenin 7-O-glucuronide from the flowers of *Asteracantha longifolia* nees, Indian Drugs 19 (1982) 150–152.

[45] A. Patra, S. Jha, P.N. Murthy, G. Manik, A. Sharone, Isolation and characterization of stigmast-5-en-3β-ol (β-sitosterol) from the leaves of *Hygrophila spinosa* T. Anders, IJPSR 1 (2010) 95–100.

[46] K.R. Khandelwal, Practical Pharmacognosy, twentieth ed., Nirali Prakashan, Pune, 2010.

[47] J.B. Harborne, Phytochemical Methods: A Guide to Modern Techniques of Plant Analysis, Springer, Rajkamal Electric Press, 1998.

[48] R. Madaan, G. Bansal, S. Kumar, A. Sharma, Estimation of total phenols and flavonoids in extracts of *Actaea spicata* roots and antioxidant studies, Indian J. Pharmaceut. Sci. 73 (2011) 666–669.

[49] G.I. Harisa, S.M. Attia, K.M.A. Zoheir, F.K. Alanazi, Chitosan treatment abrogates hypercholesterolemia-induced erythrocyte's arginase activation, Saudi Pharmaceut. J. 25 (2017) 120–127.

[50] A. Patra, S. Satpathy, A.K. Shenoy, J.A. Bush, M. Kazi, M.D. Hussain, Formulation and evaluation of mixed polymeric micelles of quercetin for treatment of breast, ovarian, and multidrug resistant cancers, Int. J. Nanomed. 13 (2018) 2869–2881.

[51] H. Duan, D. Wang, Y. Li, Green chemistry for nanoparticle synthesis, Chem. Soc. Rev. 44 (2015) 5778–5792.

[52] H.Y. El-Kassas, M.M. El-Sheekh, Cytotoxic activity of biosynthesized gold nanoparticles with an extract of the red seaweed *Corallina officinalis* on the MCF-7 human breast cancer cell line, Asian Pac. J. Cancer Prev. APJCP 15 (2014) 4311–4317.

[53] D. Philip, C. Unni, S.A. Aromal, V.K. Vidhu, *Murraya Koenigii* leaf-assisted rapid green synthesis of silver and gold nanoparticles, Spectrochim. Acta Part A Mol. Biomol. Spectrosc. 78 (2011) 899–904.

[54] M.A. Rahman, A. Hussain, Anti-cancer activity and apoptosis inducing effect of methanolic extract of *Cordia dichotoma* against human cancer cell line, Bangladesh, J. Pharmacol. 10 (2015) 27–34.

[55] A.R. Ndhlala, M. Moyo, J. Van Staden, Natural antioxidants: fascinating or mythical biomolecules, Molecules 15 (2010) 6905–6930.

[56] H.R. Siddique, M. Saleem, Beneficial health effects of lupeol triterpene: a review of preclinical studies, Life Sci. 88 (2011) 285–293.

[57] M.B.C. Gallo, M.J. Sarachine, Biological activities of lupeol, Int. J. Biomed. Pharmaceut. Sci. 3 (2009) 46–66.

[58] Z.E.J. Perez, R. Mathiyalagan, J. Markus, Y.J. Kim, H.M. Kang, R. Abbai, K. Seo, D. Wang, V. Soshnikova, D.C. Yang, Ginseng-berry-mediated gold and silver nanoparticle synthesis and evaluation of their in vitro antioxidant, antimicrobial, and cytotoxicity effects on human dermal fibroblast and murine melanoma skin cell lines, Int. J. Nanomed. 12 (2017) 709–723.

[59] C. Wang, R. Mathiyalagan, Y.J. Kim, V. Castro-Aceituno, P. Singh, S. Ahn, W. Dandan, D.C. Yang, Rapid green synthesis of silver and gold nanoparticles using *Dendropanax morbifera* leaf extract and their anticancer activities, Int. J. Nanomed. 11 (2016) 3691–3701.

[60] M. Hamelian, K. Varmira, H. Veisi, Green synthesis and characterizations of gold nanoparticles using Thyme and survey cytotoxic effect, antibacterial and antioxidant potential, J. Photochem. Photobiol., B 184 (2018) 71–79.

[61] C.G. Yuan, C. Huo, S. Yu, B. Gui, Biosynthesis of gold nanoparticles using *Capsicum annuum* var. *grossum* pulp extract and its catalytic activity, Physica E 85 (2017) 19–26.

[62] Y. Qu, X. pei, W. Shen, X. Zhang, J. Wang, Z. Zhang, S. Li, S. You, F. Ma, J. Zhou, Biosynthesis of gold nanoparticles by Aspergillum sp. WL-Au for degradation of aromatic pollutants, Physica E 88 (2017) 133–141.

[63] N.U. Islam, R. Amin, M. Shahid, M. Amin, Gummy gold and silver nanoparticles of apricot (*Prunus armeniaca*) confer high stability and biological activity, Arab. J. Chem. DOI:10.1016/j.arabjc.2016.02.017.

[64] S. Sarker, L. Nahar, Natural medicine: the genus Angelica, Curr. Med. Chem. 11 (2004) 1479–1500.

[65] S. Honary, F. Zahir, Effect of zeta potential on the properties of nano-drug delivery systems - a review (Part 2), Trop. J. Pharmaceut. Res. 12 (2013) 265–273.

[66] B. Paul, B. Bhuyan, D.D. Purkayastha, D. Madhudeepa, S.S. Dhar, Greens Synthesis of gold nanoparticle using *Pogestemon benghalensis* (B) O. Ktz. Leaf extract and studies of their photocatalytic activity in degradation of methylene blue, Mater. Lett. 148 (2015) 37–40.

[67] C. Singh, R.K. Baboota, P.K. Naik, H. Singh, Biocompatible synthesis of silver and gold nanoparticles using leaf extract of *Dalbergia sissoo*, Adv. Mat. Lett. 3 (2012) 4–13.

[68] Y.H. Jeong, S.Y. Chung, A.R. Han, M.K. Sung, D.S. Jang, J. Lee, Y. Kwon, H.J. Lee, E.K. Seo, P-glycoprotein inhibitory activity of two phenolic compounds, (-)-syringaresinol and tricin from *Sasa borealis*, Chem. Biodivers. 4 (2007) 12–16.

[69] C.P. Rubio, J. Hernandez-Ruiz, S. Martinez-Subiela, A. Tvarijonaviciute, J.J. Ceron, Spectrophotometric assays for total antioxidant capacity (TAC) in dog serum: an update, BMC Vet. Res. 12 (2016) 166, https://doi.org/10.1186/s12917-016-0792-7.

[70] M.D. Hussain, M. Ogbuechi, Safety and toxicity of nanoparticles in medicine, in: R. Sethi, C. Kolli, M.D. Hussain (Eds.), Toxicology: the Past, Present and Future of Basic, Clinical and Forensic Medicine, Nova Science Publishers, Inc., New York, 2015, pp. 45–67.

[71] M. Misawa, J. Takahashi, Generation of reactive oxygen species induced by gold nanoparticles under x-ray and UV irradiations, Nanomedicine 7 (2011) 604–614.

[72] R. Govindarajan, M. Vijaykumar, P. Pushpangadan, Antioxidant approach to disease management and the role of 'Rasayana' herbs of Ayurveda, J. Ethnopharmacol. 99 (2005) 165–178.
[73] V. Hajhashemi, G. Vaseghi, M. Pourfarzam, A. Abdollahi, Are antioxidants helpful for disease prevention, Res. Pharm. Sci. 5 (2010) 1–8.
[74] A.A. Gabizon, Selective tumor localization and improved therapeutic index of anthracyclines encapsulated in long-circulating liposomes, Canc. Res. 52 (1992) 891–896.